

Cloud vertical distribution from radiosonde, remote sensing, and model simulations

Jinqiang Zhang · Zhanqing Li · Hongbin Chen ·
Hyelim Yoo · Maureen Cribb

Received: 8 April 2013 / Accepted: 15 April 2014 / Published online: 7 May 2014
© Springer-Verlag Berlin Heidelberg 2014

Abstract Knowledge of cloud vertical structure is important for meteorological and climate studies due to the impact of clouds on both the Earth's radiation budget and atmospheric adiabatic heating. Yet it is among the most difficult quantities to observe. In this study, we develop a long-term (10 years) radiosonde-based cloud profile product over the Southern Great Plains and along with ground-based and space-borne remote sensing products, use it to evaluate cloud layer distributions simulated by the National Centers for Environmental Prediction global forecast system (GFS) model. The primary objective of this study is to identify advantages and limitations associated with different cloud layer detection methods and model simulations. Cloud occurrence frequencies are evaluated on monthly, annual, and seasonal scales. Cloud vertical distributions from all datasets are bimodal with a lower peak located in

the boundary layer and an upper peak located in the high troposphere. In general, radiosonde low-level cloud retrievals bear close resemblance to the ground-based remote sensing product in terms of their variability and gross spatial patterns. The ground-based remote sensing approach tends to underestimate high clouds relative to the radiosonde-based estimation and satellite products which tend to underestimate low clouds. As such, caution must be exercised to use any single product. Overall, the GFS model simulates less low-level and more high-level clouds than observations. In terms of total cloud cover, GFS model simulations agree fairly well with the ground-based remote sensing product. A large wet bias is revealed in GFS-simulated relative humidity fields at high levels in the atmosphere.

Keywords Cloud vertical structure · NCEP global forecast system · Radiosonde · Cloud fraction · Remote sensing

This paper is a contribution to the Topical Collection on Climate Forecast System Version 2 (CFSv2). CFSv2 is a coupled global climate model and was implemented by National Centers for Environmental Prediction (NCEP) in seasonal forecasting operations in March 2011. This Topical Collection is coordinated by Jin Huang, Arun Kumar, Jim Kinter and Annarita Mariotti.

J. Zhang · H. Chen
Key Laboratory of Middle Atmosphere and Global Environment
Observation, Institute of Atmospheric Physics, Chinese
Academy of Sciences, Beijing, China

Z. Li
College of Global Change and Earth System Sciences,
Beijing Normal University, Beijing, China

Z. Li (✉) · H. Yoo · M. Cribb
Department of Atmospheric and Oceanic Science, Earth System
Science Interdisciplinary Center, University of Maryland,
College Park, MD, USA
e-mail: zli@atmos.umd.edu

1 Introduction

Cloud vertical structure affects, and is affected by, atmospheric dynamics, thermodynamics, and the hydrological cycle, as well as the radiation budget at the surface and within the atmosphere. Clouds have been recognized as a primary source of uncertainties in global weather and climate studies (Stephens 2005). By comparing 24 model simulations against International Satellite Cloud Climatology Project (ISCCP) data, Weare (1996) found that global mean amounts of modeled high clouds were about two to five times greater than that calculated from satellite retrievals, whereas low-level clouds were severely underestimated. Zhang et al. (2005) compared the fraction of

total, low-level, mid-level, and high-level clouds from 10 general circulation models (GCMs) and the ISCCP satellite product, as well as the clouds and earth's radiant energy system (CERES) cloud product. They showed that total cloud amounts agreed well. However, large discrepancies existed in cloud vertical structure among the models, and between satellite products.

Validation of climate models requires an accurate knowledge of cloud macrophysical properties from observational data. Passive satellite sensors have the advantage of providing a global coverage of cloud amounts and top heights, but their retrieval accuracy suffers from various limitations (Marchand et al. 2001). Ground-based active sensors, such as cloud radars, lidars, and ceilometers, can provide cloud property measurements with high accuracy and with continuous temporal coverage (Dong and Mace 2003; Okamoto et al. 2008; Xi et al. 2010). The advent of the space-borne cloud radar and lidar allows for the portrayal of cloud vertical structure on a global scale along the curtain of a satellite track due to its nadir view mode (Stephens et al. 2002; Mace et al. 2009).

To produce a more reliable cloud climatology, the US Department of Energy's Atmospheric Radiation Measurement (ARM) program has deployed a suite of remote sensing instruments at the Southern Great Plains (SGP) central facility (CF) site in north-central Oklahoma. By combining data from different instruments, cloud vertical structure information has been generated and is available as an active remote sensing of cloud (ARSCL) value-added product (VAP; Clothiaux et al. 2000). This VAP has been used in various studies (Dong et al. 2006; Kollias et al. 2007; Xi et al. 2010). Mace and Benson (2008) confirmed that the vertical profile of cloud occurrence was dominated by clouds in the upper troposphere and in the boundary layer, which is consistent with a global satellite cloud product (Chang and Li 2005a) derived from moderate resolution imaging spectroradiometer (MODIS) channels using their own algorithm (Chang and Li 2005b).

Using ground-based and space-borne remote sensing cloud products at the SGP site, many studies have been conducted to evaluate, test, and improve numerical models at different scales, ranging from GCMs to cloud-resolving models (e.g., Xie and Zhang 2000; Xu et al. 2002; Luo et al. 2003; Dupont et al. 2011; Qian et al. 2012). Luo et al. (2005) used ARM observations collected at the SGP CF in June and July 1997 and cloud-resolving model simulations to evaluate the representation of cirrus clouds in a single-column version of the National Centers for Environmental Prediction (NCEP) global forecast system (GFS). Yang et al. (2006) compared diurnal distributions of cloud fraction derived from the two approaches. By investigating global distributions of high, middle, and low-level cloud fractions estimated from CloudSat-Cloud-Aerosol Lidar

and Infrared Pathfinder Satellite Observations (CALIPSO) merged data, retrievals obtained from the application of the Chang and Li (2005b) algorithm to MODIS data, and from GFS model simulations, Yoo and Li (2012) found that the GFS model produced more high and middle-level clouds than the two satellite retrievals, although gross spatial patterns from the model and observations bore a close resemblance. Large discrepancies were also exhibited in marine stratocumulus clouds over the eastern tropical Pacific and Atlantic oceans, including the west coasts of North America, South America, and southwestern Africa. Yoo et al. (2013) found that the parameterization of cloudiness was the primary cause for the systematic discrepancies. The current study focuses on the SGP CF site and extends the Yang et al. (2006) study period to 10 years, but uses independent datasets of cloud structure estimated from radiosonde and ground-based retrievals. In addition, the cloud product derived from measurements made from CloudSat and CALIPSO satellites between 2006 and 2010 are also used to investigate differences in cloud retrievals, especially for high clouds. New utilities of these conventional and operational measurements are demonstrated.

World-wide radiosonde data have been obtained routinely for many decades. Radiosondes provide in situ measurements of temperature and humidity that may convey information about clouds. To take advantage of the global long-term database of radiosonde profiles, methods have been developed to determine the locations and boundaries of cloud layers from radiosonde data. Wang and Rossow (1995; denoted as WR95) used relative humidity (RH) profiles to obtain cloud vertical structure with a transformation of RH to that with respect to ice at levels where the temperature is below 0 °C. Chernykh and Eskridge (1996) developed a cloud detection method based on the second-order derivatives of temperature and RH with respect to height. Cloud boundaries are defined if at least one of the two second-order derivatives is zero. Using radiosonde data, cloud vertical structure was determined (e.g., Wang et al. 1999, 2000; Chernykh et al. 2000; Minnis et al. 2005), but few such products have been validated due to a lack of trustworthy and/or independent products (e.g., Wang et al. 1999; Naud et al. 2003).

As part of a major US–China joint experiment called the East Asian Study of tropospheric aerosols and their impact on regional climate (Li et al. 2010, 2011), an ARM mobile facility (AMF) was deployed in China. Using a modified version of the method described by WR95, radiosonde data obtained from the AMF campaign were used to analyze cloud distributions at a site in southeastern China (Zhang et al. 2010). Radiosonde-derived and W-band (95 GHz) cloud radar retrievals of cloud boundaries agreed well. The same method was also validated at the SGP site with promising accuracy (Zhang et al. 2013).

Comparative studies between the GFS and remote sensing products have been presented in Yoo and Li (2012) and Yoo et al. (2013), while the radiosonde-based cloud boundary algorithm and a preliminary validation of radiosonde-based cloud products have been presented in Zhang et al. (2010, 2013). The success achieved in using radiosonde data to determine the presence of cloud in any atmospheric layer motivated us develop a 10-year climatology of cloud vertical structure using data from radiosondes launched over the SGP CF. Radiosonde and remotely sensed cloud data have respective advantages and limitations. Yet, space-borne and ground-based remote sensing products also have different merits and limitations (Thorsen et al. 2013; Protat et al. 2014). In this regard, no single product can be regarded as the truth. As such, they are all used to evaluate the performance of the National Oceanic and Atmospheric Administration (NOAA)/GFS in simulating cloud vertical profiles. Four products (GFS, ground- and space-based remotely sensed products, and radiosonde) are employed here that were generated over many years to study the climatology of cloud profiles, as well as to investigate their differences. This is part of a series of comprehensive investigation with some results already published (Yoo and Li 2012; Yoo et al. 2013; Zhang et al. 2010, 2013).

Section 2 describes the cloud detection algorithms and data used in this study. Cloud occurrence frequencies from observations and model simulations at the SGP site are compared in Sect. 3. Differences are also investigated. Main conclusions are summarized in Sect. 4.

2 Cloud detection algorithms and data

2.1 Radiosonde-based method and product

At the SGP site, a minimum of four radiosonde launches are launched each day (at 05:30, 11:30, 17:30, and 23:30 UTC). More frequent launches were made during numerous intensive field campaigns that took place at the site, such as the Atmospheric Infrared Sounder Campaign (Tobin et al. 2006) and the Cloud Land Surface Interaction Campaign (Miller 2008). Radiosonde data collected at the SGP site from 2001 to 2010 are used to derive cloud layers in this study using the algorithm described by Zhang et al. (2013).

A brief introduction is presented here for completeness. The algorithm originates from that described by WR95 with numerous modifications. It employs three height-resolving RH thresholds to determine cloud layers: minimum and maximum RH thresholds in cloud layers (min-RH and max-RH), and minimum RH thresholds within the distance between two contiguous layers (inter-RH). RH is

first computed with respect to ice instead of liquid water at all levels with temperatures below 0 °C. Cloud layers are then identified according to the following eight steps: (1) the base of the lowest moist layer is determined as the level where RH exceeds the min-RH corresponding to this level; (2) levels above the base of the moist layer with RH greater than the min-RH are treated as the same layer; (3) the top of the moist layer is identified where RH decreases to the min-RH or RH exceeds the min-RH, but the top of the profile is reached; (4) the moist layer is classified as a cloud layer if the maximum RH within this layer is higher than the corresponding max-RH at the base of this moist layer; (5) the base of cloud layers is set to 136 m above ground level (AGL); (6) two neighboring cloud layers are considered as a one-layer cloud if the distance between these two layers is less than 300 m or the minimum RH within this distance is greater than the maximum inter-RH value within this distance; (7) if no cloud layers are identified below 1 km where a large RH change gradient occurred ($>15\%$ RH/km) and the maximum RH exceeds 85 %, one cloud layer is determined; and (8) clouds are discarded if their thicknesses are less than 30.5 m for low clouds and 61 m for middle/high clouds.

2.2 Ground-based cloud detection algorithm and products

Ground-based active remote sensors such as the millimeter microwave cloud radar (MMCR; Moran et al. 1998; Miller et al. 2003) are capable of detecting multiple cloud layers with high temporal and vertical resolutions so can provide detailed information on cloud layer overlap. The MMCR operates in four modes (Clothiaux et al. 1999) to provide continuous profiles of radar reflectivity by hydrometeors within its field of view. The laser ceilometer and lidar are sensitive to the second moment of the particle distribution; however, the MMCR is sensitive to the sixth moment so it can readily detect non-hydrometeors associated with insects and bits of vegetation. Thus, the ceilometer and lidar can provide a more reliable estimate of cloud-base height than can the MMCR. By combining observations from the cloud radar, the lidar, and the ceilometer, the ARSCL VAP was generated to detect cloud boundaries with the best possible accuracy (Clothiaux et al. 2000; Kollias et al. 2009). The ARSCL VAP generated at the SGP site between 2001 and 2010 is used in this study.

2.3 The GFS model

The NCEP GFS is a global weather prediction model run by NOAA. The GFS model is based on primitive dynamical equations including a few parameterizations for atmospheric physics developed by Sela (1980) and

Kanamitsu (1989). The GFS model outputs cloud fraction, cloud-top pressure and temperature, and cloud-base pressure and temperature at high, middle and low levels of the atmosphere. The GFS cloud fraction is diagnostically calculated based on a prognostic condensate scheme which combines the model-predicted temperature, RH, and three-dimensional cloud water mixing ratios (Xu and Randall 1996). The GFS model has 64 vertical sigma-pressure hybrid layers and outputs parameters in 21 vertically different layers. From the surface (1,000 hPa) to the 900 hPa level, the vertical resolution is 25 hPa; above 900 hPa, there are 16 levels at a 50-hPa resolution.

National Centers for Environmental Prediction GFS forecast data have been processed since 2001 to produce model profiles of atmospheric and cloud variables at ARM observation sites two times per day, initialized at 0000 UTC and 1,200 UTC (Yang et al. 2006). ARM sites include the SGP site near Lamont, Oklahoma, the North Slope of Alaska, and the Tropical Western Pacific. Standard model variables such as surface and atmospheric temperatures, cloud fraction, cloud condensates, and specific humidity are extracted and archived at 3-h forecast intervals. The forecast duration is from the control time of 0000 UTC to 48 h later. The saturation specific humidity is transformed with respect to liquid or ice phase depending on the ambient temperature. To compare with observational data, GFS output profiles were saved on the model's sigma levels and then projected onto standard isobaric layers from 1,000 to 25 hPa with a 25-hPa solution. Model output is also generated at atmospheric heights ranging from the surface to 20 km spaced at 250-m interval. Forecast data from 00 UTC to 24 UTC (i.e. at 03, 06, 09, 12, 15, 18, 21, 24 UTC) for each day between January 2001 and July 2010 are used in this study.

2.4 Space-borne cloud detection algorithm and products

The space-borne cloud data used in this study is the 2B-GEOPROF-LIDAR product derived from CloudSat and CALIPSO satellites. The two satellites were launched in 2006 and carry a 94-GHz cloud profiling radar (Stephens et al. 2002) and a two-wavelength polarization sensitive lidar (Winker et al. 2007). The lidar is able to detect thin cirrus, but is attenuated by optically thick clouds. However, the radar is able to detect lower, more optically opaque cirrus clouds and can penetrate through much of deep convective clouds. Similar to ground-based ARSCL VAP data, the combination of space-borne lidar and radar data offers the best compromise between the strengths and weaknesses of the two instrument retrieval methods (Mace et al. 2009). It thus allows for a more complete description of the cloud vertical structure; the boundaries of up to five

cloud layers can be identified. The 2B-GEOPROF-LIDAR product generated between 2006 and 2010 over the SGP site is used in this study.

3 Comparison of cloud layers derived at the SGP site

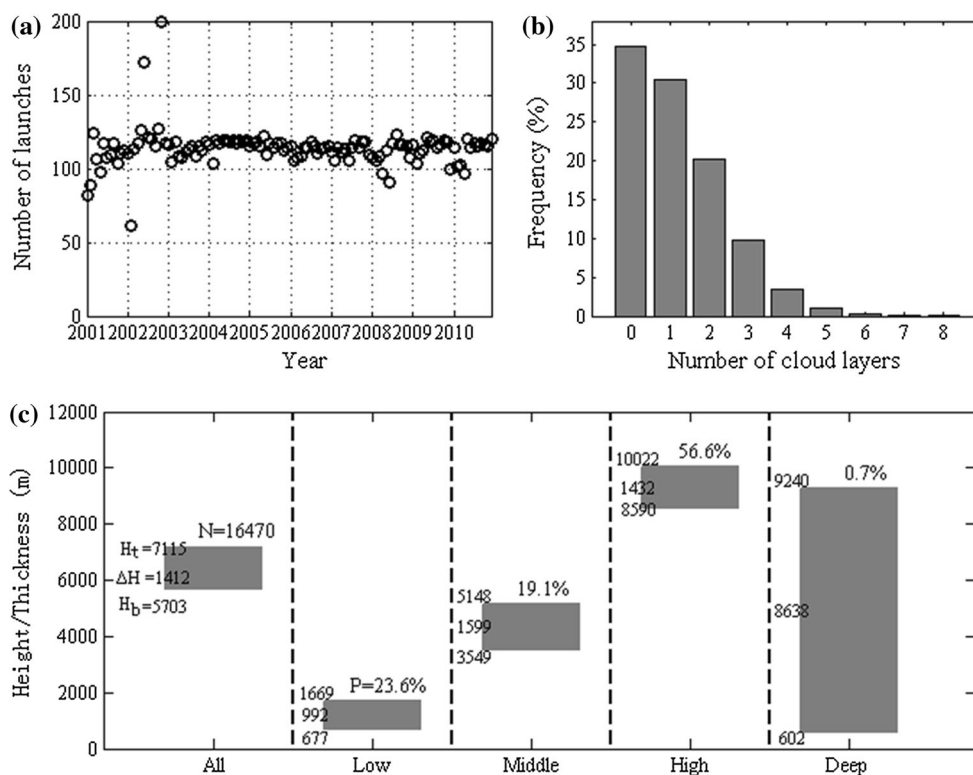
3.1 Radiosonde-derived cloud layer statistics

Radiosonde profiles reaching altitudes greater than 10 km over the period of 2001–2010 were selected, resulting in a total of 13,635 profiles. Monthly samples exceed 100 for 94 % of the months (Fig. 1a). Frequency distributions of the number of radiosonde-detected cloud layers are shown in Fig. 1b. Clear skies were most frequently observed (34.8 % of the cases), followed by skies with one layer of cloud (30.4 %) and two layers of cloud (20.2 %). A maximum of eight cloud layers was detected during the course of one particular launch. A total of 16,470 cloud layers were retrieved and were classified according to their location in the atmosphere: (1) low clouds with bases lower than 2 km and thicknesses less than 6 km; (2) mid-level clouds with bases ranging from 2 to 5 km; (3) high clouds with bases greater than 5 km (Lazarus et al. 2000), and (4) deep clouds with bases less than 2 km and thicknesses greater than 6 km. The mean location for each cloud type is presented in Fig. 1c. The mean cloud-base height, cloud-top height, and thickness for all cloud layers are 5,703, 7,115 and 1,412 m, respectively. Of all cloud layers detected, 23.6, 19.1, 56.6, and 0.7 % are low, mid-level, high and deep clouds, respectively. Low-level clouds are thinnest with a mean thickness of 992 m and deep clouds are thickest (8,638 m); mid-level clouds tend to be thicker than high-level clouds.

3.2 Cloud occurrence frequency comparisons

Clouds in different vertical layers dictate the adiabatic heating rate and the radiation balance of the atmospheric column. Ten years' worth of radiosonde, ARSCL, and GFS data at the SGP site allows for the analysis of cloud occurrence frequencies on different temporal scales (monthly, yearly, and seasonally) and the comparison of cloud results derived from these three datasets. The radiosonde-derived cloud occurrence frequency is defined as the number of launches where at least one layer of cloud was detected divided by the total number of radiosonde launches during a certain period (e.g., a month). Cloud occurrence frequencies generated at the time of radiosonde launches are used in the comparisons of subsequent analyses, which are defined as the number of samples where cloud layers were detected divided by the total number of samples in the ARSCL subset of retrievals during a certain

Fig. 1 **a** Monthly number of selected radiosonde launches, **b** the frequency distribution of the number of radiosonde-retrieved cloud layers, and **c** mean locations for all-cloud layers, and low-/mid-/high-level clouds and deep clouds. H_b , H_t , and ΔH (unit: m) are the mean cloud-base height, top height, and thickness for each type of clouds, respectively. N denotes the total number of cloud layers detected at the SGP site, and P is the percentage of each cloud type out of all cloud layers



period. Note that there are differences between the frequencies of cloud occurrence at the times of radiosonde launches and from all day long due to the diurnal cycle of cloud occurrence (Dong et al. 2006; Zhang and Klein 2010). GFS-based clouds are derived by applying the radiosonde cloud retrieval algorithm to the GFS model-predicted RH field (GFS-RH). The GFS-RH-based cloud occurrence frequency is defined in the same way as that used for radiosonde retrievals.

The 10-year radiosonde-based (ARSCL) mean cloud occurrence frequencies for all-clouds, low-, middle-, high-, and deep clouds at the SGP site are 65 % (52 %), 26 % (20 %), 20 % (14 %), 47 % (31 %), and 1 % (2 %), respectively (see Table 1). Cloud occurrence frequencies calculated here using radiosonde data are larger than those reported by others using ARSCL retrievals (Dong et al. 2006; Kollias et al. 2007; Mace and Benson 2008; Xi et al. 2010). There are three major factors that may explain the discrepancies between the two observational data sets. One factor involves balloon drift (Zhang et al. 2013). Balloon drift distances are generally more than 20 km with a maximum of about 200 km. Another factor is the different temporal resolutions of the data sets. The temporal resolution of data used in the published studies is either 5 min or 10 s. However, during a radiosonde launch, the instrument generally spends more than 90 min in the atmosphere collecting data. As noted by Xi et al. (2010) and Kennedy et al. (2010), the cloud occurrence

frequency will increase as the sampling period, or area, increases. Radiosondes travel through the troposphere for about 45 min, so more clouds are observed than are seen in the ARSCL product. The radiosonde-retrieved mean cloud occurrence frequency of 65 % is on par with the red dot in Fig. 1 of Xi et al. (2010), which is equivalent to satellite observations made over a $0.5^\circ \times 0.5^\circ$ box centered on the SGP CF or 30–45 min of point observations. The other factor involves the macro- and microphysical nature of lower-level cloud layers. Ground-based instruments may fail to detect some high cirrus due to the attenuation effect of thick lower-level clouds and fog on the instruments (Protat et al. 2014). This will be addressed later. The frequency occurrence of GFS-based clouds is generally smaller than that from radiosonde retrievals, which is associated with how often data were generated. GFS-modeled RH is output at 3-h intervals while radiosonde profiles are generated every 6 h. In terms of total cloud cover, GFS model simulations agree fairly well with the ground-based remote sensing product.

3.2.1 Annual variations in cloud occurrence frequency

Time series (2001–2010) of annual cloud occurrence frequencies for all-clouds, low-level, mid-level, high-level, and deep clouds derived from radiosonde, ARSCL, and GFS data are shown in Fig. 2. The radiosonde-based cloud occurrence frequency (Fig. 2a) for all-clouds varies

Table 1 Mean cloud occurrence frequencies and standard deviations calculated from radiosonde, ARSCL, and GFS data, averaged over 2001–2010 for all clouds and four different cloud types

	Cloud occurrence frequency (%)			Standard deviation (%)		
	Radiosonde	ARSCL	GFS	Radiosonde	ARSCL	GFS
All clouds	65	52	58	11	13	12
Low clouds	26	20	16	13	11	9
Middle clouds	20	14	9	7	5	4
High clouds	47	31	43	9	9	11
Deep clouds	1	2	2	1	2	2

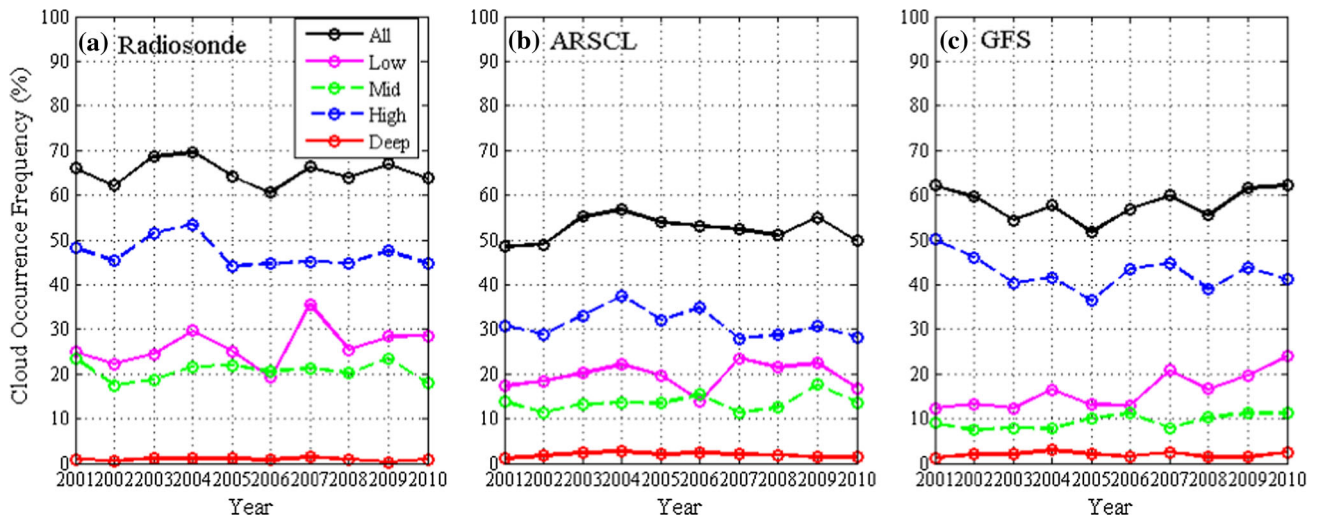


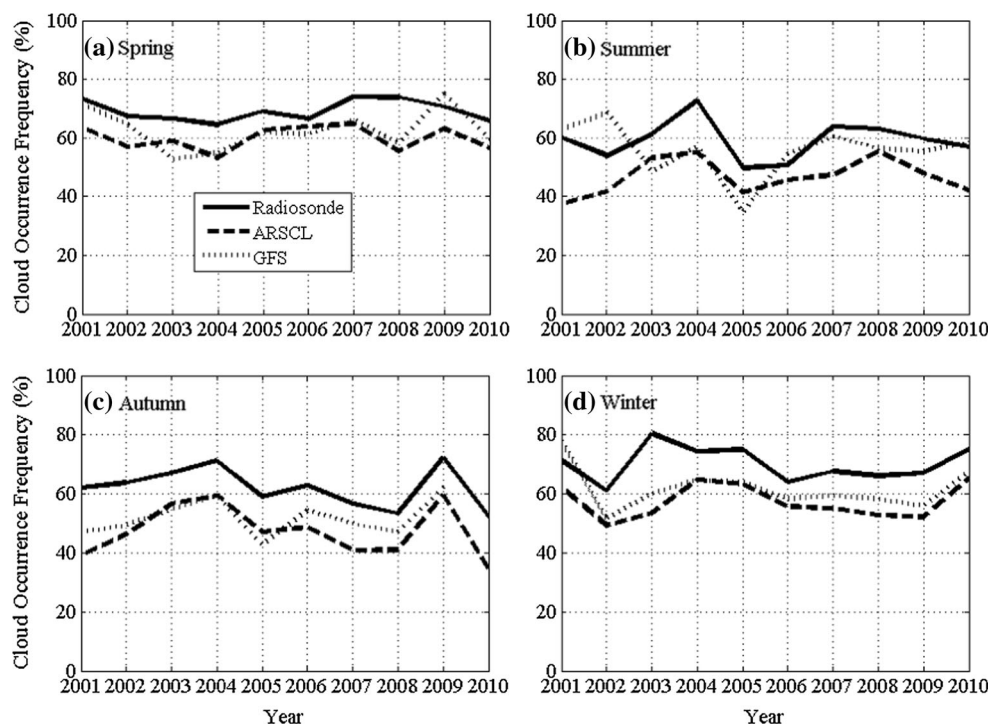
Fig. 2 Annual mean cloud occurrence frequencies from 2001 to 2010 for all-clouds (*black line*), low- (*pink line*), mid- (*green line*), high-level clouds (*blue line*), and deep clouds (*red line*) derived from **a** radiosonde data, **b** the ARSCL product, and **c** the GFS model at the SGP site

between 60 and 70 %. The maximum frequency is 69.6 % in 2004 and the minimum is 60.6 % in 2006. The frequency of mid-level and deep clouds hovers around 20 and 1 %, respectively. The frequency of low-level clouds jumps from 19 % in 2006 to 35 % in 2007; the frequency of high-level clouds is highest over the period of 2003–2004 and varies in the same manner as all-clouds, stabilizing after 2005. The frequency trend for all-clouds derived from ARSCL (Fig. 2b) is similar to that from the radiosonde except from 2006 to 2008. Others have reported that the ARSCL-based mean frequency at the SGP site from January 1997 through December 2002 (Dong et al. 2006) and from January 1998 through June 2004 (Kollias et al. 2007) is 49 %. Xi et al. (2010) reported a value of 47 % between January 1997 and December 2006. The mean ARSCL all-cloud frequency from 2001 to 2002 (Fig. 2b) is 50 %. But for all years after 2002, it is larger than 50 %, which makes the 10-year mean frequency greater than other published values. The occurrence frequencies for all GFS-modeled clouds (Fig. 2c) tend to be less than those from radiosonde retrievals; large differences in trend are also seen in all-cloud and high-level cloud layers.

Figure 3 shows the seasonal time series of annual mean cloud occurrence frequency distributions for all clouds from Fig. 2. The four seasons are defined as follows: winter (December–February), spring (March–May), summer (June–August), and autumn (September–November). In general, more cloud layers are detected in the spring and winter than in the summer and autumn. Compared to ARSCL, the GFS simulates well the inter-annual variations of cloud occurrence in most seasons, except in the summer when the performance of the model cloud simulation deteriorated. Similar trends in inter-annual variation are observed among the three products, especially between the two observation products despite their systematic differences. The radiosonde-based cloud occurrence frequency is larger in magnitude than the ARSCL cloud occurrence frequency by about 10 %. The mean difference of radiosonde relative to instantaneous cloud frequency of ARSCL is 9.3, 12.5, 14.8, and 12.8 % in spring, summer, autumn, and winter, respectively. The mean bias over the four seasons is 12.6 %.

Annual mean cloud occurrence frequencies at a vertical resolution of 100 m are shown in Fig. 4. The color bar represents the cloud occurrence frequencies in percent.

Fig. 3 Annual mean distributions of cloud occurrence frequency at the SGP site obtained from radiosonde profiles (*solid lines*), the ARSCL product (*long dashed lines*), and the GFS model (*short dashed lines*) in **a** spring, **b** summer, **c** autumn, and **d** winter



Cloud-top heights and their standard deviations for low-/mid-/high-level clouds are also shown. The radiosonde- and GFS-based vertical cloud occurrence frequencies in each 100-m bin is defined as the number of times a cloud or portion of cloud was detected in that bin divided by the total number of vertical profiles during the month or year in question. The ARSCL-based vertical cloud occurrence frequency is defined in a similar way, i.e., the number of samples detecting cloud layers anywhere within a specified 100-m bin divided by the total number of samples during the month or year in question.

In general, the distribution of radiosonde-derived clouds (Fig. 4a) over the SGP site is characterized by more clouds located in the upper and lower atmosphere and relatively fewer mid-level clouds, which seems to be a global gross feature as found by Chang and Li (2005b). The largest number of boundary-layer clouds occurred in 2007; cirrus clouds abounded in 2001, 2003, and 2004. Figures 2a and 4a show that the lowest frequency of radiosonde-derived low-level clouds seen in 2006 ($\sim 20\%$) corresponded to a period when there was a lower-than-normal number of such clouds within the boundary layer; the highest frequency of clouds seen in 2004 ($\sim 70\%$) corresponded to a period when there was a greater-than-normal number of clouds in the upper atmosphere. Overall, vertical distributions of cloud derived from the ARSCL (Fig. 4b) are about 10% less than those from the radiosonde at many levels in the atmosphere. Cloud-top heights are similar in Fig. 4a, b; they vary slightly around their mean values, as illustrated in Fig. 1c. Compared to radiosonde and ARSCL retrievals,

many more high-cloud layers are simulated by the GFS model (Fig. 4c), resulting in the largest values for cloud-top height of high clouds. The cloud-top height of mid-level clouds varies the most between 2004 and 2007. Less boundary-layer clouds are generated by the GFS model than measured by radiosondes.

Figure 5 shows average profiles of RH and temperature derived from radiosonde data and the GFS model over the 10-year period. In general, temperatures obtained from the two approaches are very close. However, large discrepancies are revealed in the RH profiles. There exists a wet bias in GFS-modeled RH, especially in the upper atmosphere. The deficiency in GFS-modeled low-level cloud layers may be partially associated with the coarser vertical resolution of the model (250 m) compared to that of radiosonde measurements (10 m). This may result in a few thin cloud layers being missed by the GFS model near the surface. More cloud layers from the GFS model in the upper atmosphere are presumably due to the large wet bias at these levels, which can lead to a positive bias in cloud ice. To obtain more accurate cloud boundaries, GFS-RH thresholds used to determine the cloud field should be increased (decreased) in the upper (lower) part of the atmosphere.

3.2.2 Monthly variations in cloud occurrence frequency

Figure 6 shows the monthly mean time series of the vertical distribution of radiosonde-derived, ARSCL-retrieved, and GFS-modeled cloud occurrence frequencies over the

Fig. 4 Annual mean vertical distributions of cloud occurrence frequency derived from **a** radiosonde data, **b** the ARSCL product, and **c** GFS model output at the SGP site. The vertical resolution is 100 m. The *color bar* represents the cloud occurrence frequencies in percent. Uppermost, middle, and lowermost *white lines* represent mean cloud-top heights for high-/mid-/low-level clouds and their standard deviations, respectively

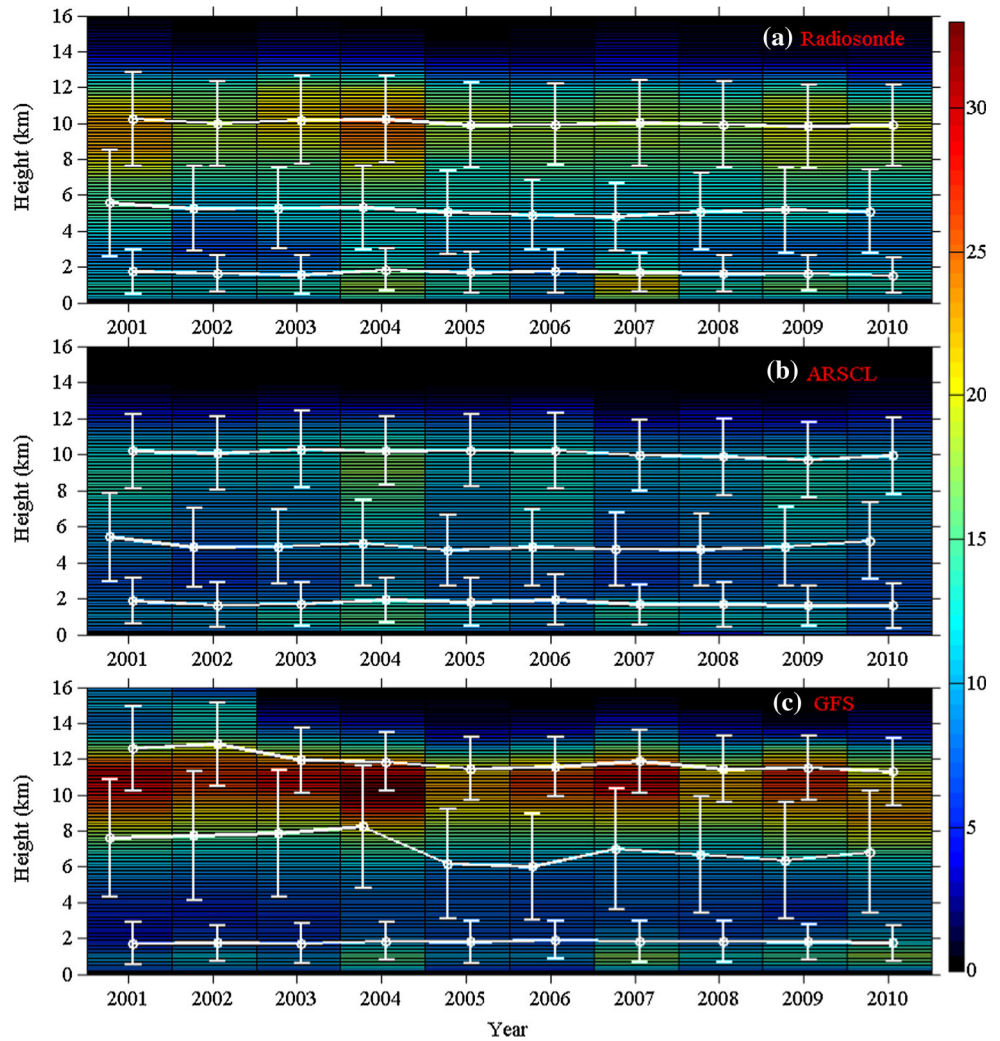
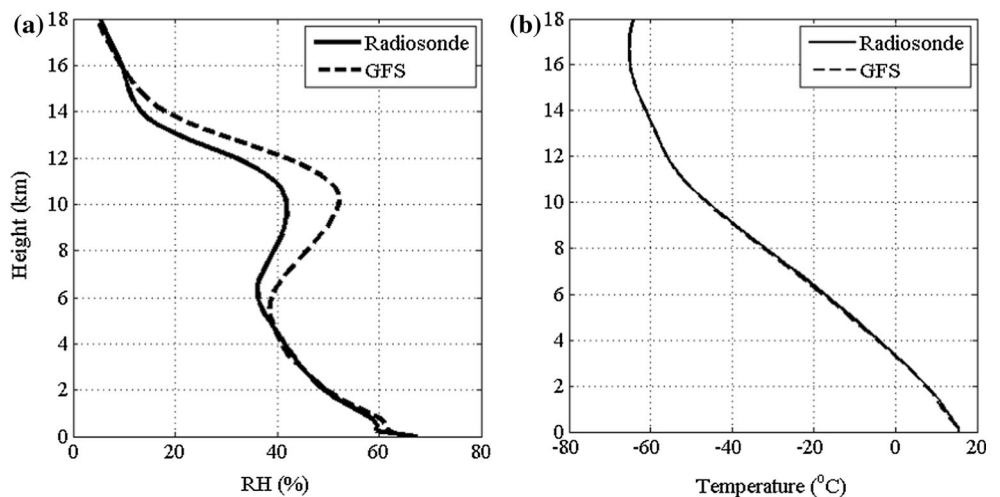


Fig. 5 Comparison of **a** relative humidity and **b** temperature derived from the radiosonde data (solid line) and from GFS model output (dashed line) at the SGP site. The vertical resolution is 250 m



10-year period studied. Most radiosonde- (Fig. 6a) and ARSCL-based (Fig. 6b) clouds are located between 8 and 12 km and the least amount of cloud is observed between 2 and 6 km in the majority of months; large month-to-month

variations are seen. The occurrence frequency below 2 km has a large monthly variability with maxima in cold months (December, January, and February) and minima in warm months (June, July, and August). The large variability in

Fig. 6 Monthly mean vertical distributions of cloud occurrence frequency derived from **a** radiosonde data, **b** the ARSCL product, and **c** the GFS model at the SGP site. The vertical resolution is 100 m. The color bar represents cloud occurrence frequencies in percent. The white band in panel **c** indicates that no GFS model simulations were available

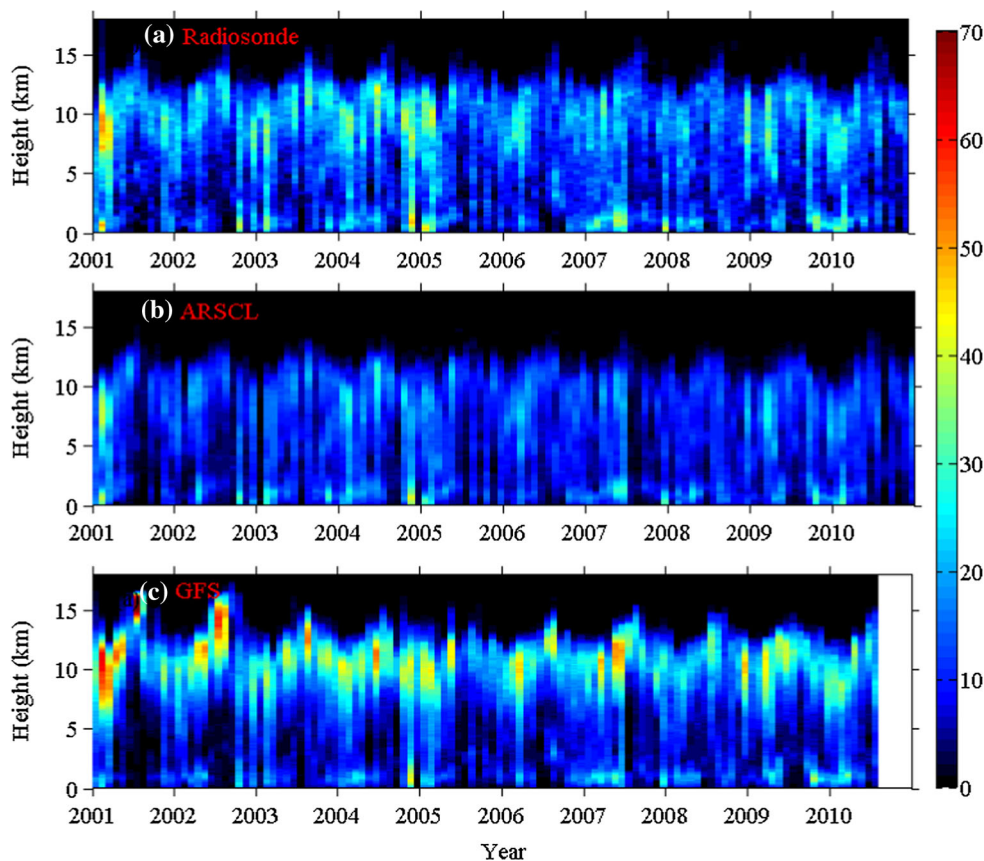


Table 2 Same as Table 1, but for all clouds and according to season

	Cloud occurrence frequency (%)			Standard deviation (%)		
	Radiosonde	ARSCL	GFS	Radiosonde	ARSCL	GFS
Spring	69	60	63	7	7	10
Summer	59	47	55	10	11	13
Autumn	62	47	52	12	14	11
Winter	71	58	61	10	13	9

boundary layer clouds and continental stratus indicates possible coupling mechanisms between the formation of continental stratus clouds and large-scale dynamics that also exhibit great variability at mid-latitudes (Kollias et al. 2007). The maximum frequency occurs in February 2001 between 7 and 11 km; cloud occurrence frequencies are generally greater than 40 % (35 %) in Fig. 6a, b. Low-level clouds derived from radiosonde profiles and generated by ARSCL vary the most on a monthly basis (13 and 11 %, respectively; see Table 1); mid-level clouds vary the least on a monthly basis (7 and 5 %, respectively). More cloud layers located above 12 km are observed by the radiosonde than are generated by the ARSCL product, especially in summer months. Substantially less low-level clouds and more high-level clouds are generated by the

GFS model (Fig. 6c) compared to radiosonde retrievals (Fig. 6a). Note that in January 2003, one of the instruments providing input to the ARSCL algorithm (the micropulse lidar) failed, therefore, no cloud boundaries were generated for this month.

3.2.3 Seasonal mean cloud occurrence frequency

Mean cloud occurrence frequencies during the four seasons and over the 10-year period at the SGP site are given in Table 2. The radiosonde-based maximum frequency occurs in winter (71 %) and the minimum frequency occurs in summer (59 %); the greatest variability in frequency occurs during the fall months (± 12 %) and the smallest variability is seen during the spring months (± 7 %).

Fig. 7 Mean vertical cloud occurrence frequency profiles from radiosonde data (*black lines*), the ARSCL product (*red lines*), and the GFS model (*blue lines*) for **a** spring, **b** summer, **c** autumn, and **d** winter over the SGP site from 2001 to 2010. The vertical resolution is 100 m

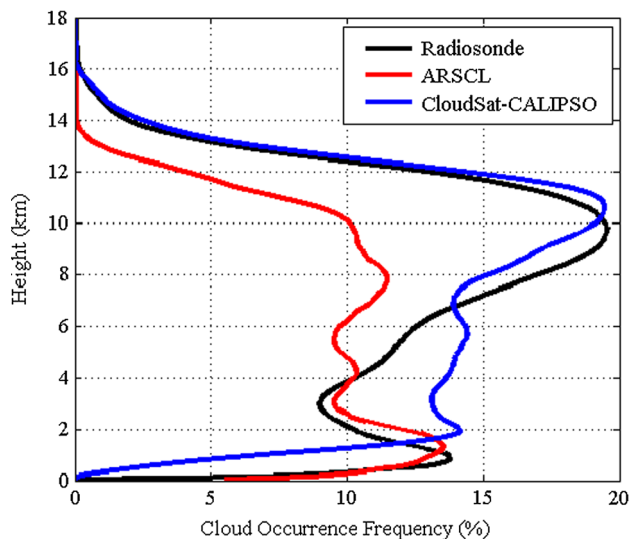
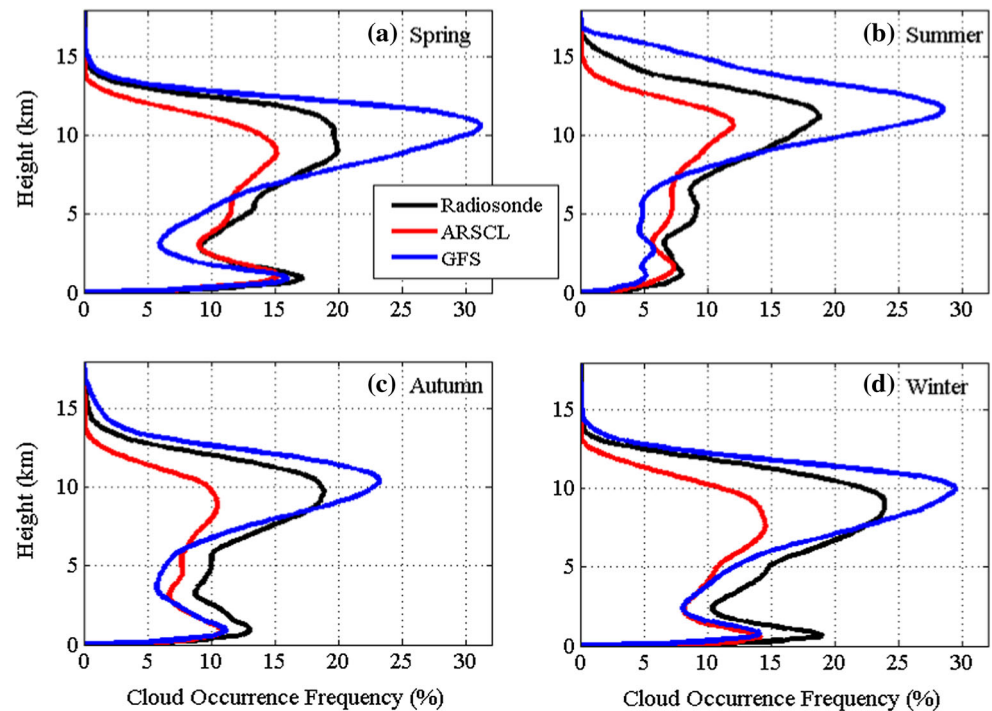


Fig. 8 A comparison of cloud occurrence frequencies calculated using the radiosonde data (*black line*), the ARSCL product (*red line*), and the CloudSat-CALIPSO combination (*blue line*) at the SGP site from 2006 to 2010. The vertical resolution is 100 m

Maxima in frequencies calculated from ARSCL data and GFS simulations occur in spring (60 and 63 %, respectively).

Mean vertical profiles of cloud occurrence frequency during the four seasons and over the 10-year period at the SGP site are shown in Fig. 7. All profiles exhibit bimodal distributions with a lower peak between 0.5 and 2 km, an upper peak between 7 and 12 km, and a minimal

occurrence of cloud at around the 3-km level. These findings are consistent with those reported by Chang and Li (2005a, b) who analyzed satellite cloud retrievals on a global scale. The uppermost peak in the summer profile (at ~ 11 km) is located higher than those in other seasons, which is due to a deeper troposphere and the more frequent occurrence of convective storms in the summer months (Xi et al. 2010). Large frequency values located below 2 km usually occur in winter, spring, and autumn but not in summer because stratus clouds are seldom seen then (Dong et al. 2005). Large differences in magnitude among the three products are seen. The magnitude of the springtime peak in cloud occurrence frequency near the surface is nearly the same for all data sets. In autumn and winter, the magnitude of the lowest peak in cloud occurrence frequency in the radiosonde-derived profile is greater than that of the other profiles. Also, a smaller number of cloud layers are simulated by the GFS model in summer. Less middle-level clouds are simulated by the GFS model in spring, summer, and autumn.

The GFS model simulates more high-level clouds and places them higher in the upper atmosphere than do radiosonde and ARSCL retrievals. The upper peak in the ARSCL profile is lower than that from the radiosonde-based profile. By comparing the CloudSat-CALIPSO merged product (within a radius of 200 km around the ground site) and ground-based data (within ± 1 h of the satellite overpass time over that area), Protat et al. (2014) found that the ground-based radar-lidar combination at Darwin, Australia could not detect most cirrus clouds

above 10 km and that the CloudSat-CALIPSO combination underreports the cloud frequency below 2 km. We have conducted a similar study here but have used data collected at the SGP site from 2006 to 2010. The space-borne vertical cloud frequency is defined in the same way as for ground-based ARSCL data. The ARSCL product misses a significant portion of high cirrus clouds compared to the satellite products (Fig. 8), which is consistent with the study by Protat et al. (2014). By contrast, the radiosonde-based detection of high clouds agrees much closely with the space-borne product. For lower clouds, radiosonde retrievals agree well with the ARSCL product; both are larger than the CloudSat-CALIPSO product. Analysis of the latter discrepancy is beyond the scope of the current investigation and will be addressed in a separate study.

4 Conclusions

As the most comprehensive field measurement facility established by the Department of Energy's ARM program in north-central Oklahoma, the SGP site is well-equipped with a large set of instruments. Three major types of cloud vertical structure datasets are compared in this study, while a cursory comparison was also made against a satellite product. They include the ARSCL VAP generated using a suite of ground-based remote sensing instruments, radiosonde-based detection of clouds that are available four times a day, and NOAA/NCEP/GFS model output. Cloud frequency, amount, and vertical distribution derived from these three data sources were first inter-compared over a 10-year period (2001–2010). The 2B-GEOPROF-LIDAR product derived from CloudSat and CALIPSO satellites are also used in conjunction with the radiosonde and ARSCL data to help understand the limitations of all cloud products.

Cloud occurrence frequencies were compared on monthly, annual and seasonal temporal scales, which helped identify advantages and limitations of different cloud data. All cloud retrievals show that clouds are predominantly located in the upper troposphere and within the boundary layer. In general, radiosonde-based low-level cloud retrievals capture the spatial patterns of hydrometers reasonably well and follow the general features seen in ground-based measurements; cloud-top heights are similar. However, radiosonde-based and space-borne occurrence frequencies of high clouds are close in magnitude and are larger than ARSCL-derived results. Compared to radiosonde and ARSCL retrievals, fewer cloud layers are detected by the GFS model within the boundary layer, which is more obvious in summer than in other seasons. The GFS-simulated upper peak in cloud occurrence frequency tends to be larger in magnitude and located higher

in the atmosphere than peaks seen from observational retrievals during all seasons. In terms of total cloud amount, GFS-model simulations agree fairly well with the ground-based remote sensing product. A large wet bias is revealed in GFS-simulated RH fields at high levels in the atmosphere. This issue should be addressed by modelers so that simulations of cloud fields can be improved.

Acknowledgments Data from the US Department of Energy's Atmospheric Radiation Measurement (ARM) Climate Research Facility located near Lamont, Oklahoma were used in this study. This work is supported by the Ministry of Science and Technology of China (2013CB955804, 2010CB950804), the National Natural Science Foundation of China under Grant 40830102, and the Office of Science of the US Department of Energy (DESC0007171).

References

- Chang FL, Li Z (2005a) A new method for detection of cirrus overlapping water clouds and determination of their optical properties. *J Atmos Sci* 62:3993–4009
- Chang FL, Li Z (2005b) A near global climatology of single-layer and overlapped clouds and their optical properties retrieved from TERRA/MODIS data using a new algorithm. *J Clim* 18:4752–4771
- Chernykh IV, Eskridge RE (1996) Determination of cloud amount and level from radiosonde soundings. *J Appl Meteorol* 35:1362–1369
- Chernykh IV, Alduchov OA, Eskridge RE (2000) Trends in low and high cloud boundaries and errors in height determination of cloud boundaries. *Bull Am Meteor Soc* 82:1941–1947
- Clothiaux EE et al (1999) The atmospheric radiation measurement program cloud radars: operational modes. *J Atmos Ocean Technol* 16:819–827. doi:10.1175/1520-0426(1999)016<0819:TARMPC>2.0.CO;2
- Clothiaux EE, Ackerman TP, Mace GG, Moran KP, Marchand RT, Miller MA, Martner BE (2000) Objective determination of cloud heights and radar reflectivities using a combination of active remote sensors at the ARM CART sites. *J Appl Meteorol* 39:645–665
- Dong X, Mace GG (2003) Arctic stratus cloud properties and radiative forcing derived from ground-based data collected near Point Barrow, Alaska. *J Clim* 16:445–461
- Dong X, Minnis P, Xi B (2005) A climatology of mid-latitude continental clouds from the ARM SGP central facility. Part I: low-level cloud macrophysical, microphysical, and radiative properties. *J Clim* 18:1391–1410
- Dong X, Xi B, Minnis P (2006) A climatology of mid-latitude continental clouds from the ARM SGP central facility. Part II: cloud fraction and surface radiative forcing. *J Clim* 19:1765–1783
- Dupont J, Haeffelin M, Morille Y, Comstock J, Flynn C, Long C, Sivaraman C, Newson R (2011) Cloud properties derived from two lidars over the ARM SGP site. *Geophys Res Lett* 38. doi:10.1029/2010GL046274
- Kanamitsu M (1989) Description of the NMC global data assimilation and forecast system. *Weather Forecast* 4:335–342
- Kennedy AD, Dong X, Xi B, Minnis P, Del Genio AD, Wolf AB, Khaiyer M (2010) Evaluation of the NASA GISS single-column model simulated clouds using combined surface and satellite observations. *J Clim* 23:5175–5192
- Kollias P, Tselioudis G, Albrecht BA (2007) Cloud climatology at the Southern Great Plains and the layer structure, drizzle, and atmospheric modes of continental stratus. *J Geophys Res* 112. doi:10.1029/2006JD007307

- Kollias P, Miller MA, Johnson KL, Jensen MP, Troyan DT (2009) Cloud, thermodynamic, and precipitation observations in West Africa during 2006. *J Geophys Res* 114. doi:10.1029/2008JD010641
- Lazarus S, Krueger SK, Mace GG (2000) A cloud climatology of the Southern Great Plains ARM CART. *J Clim* 13:1762–1775
- Li Z et al (2011) East Asian Studies of Tropospheric Aerosols and their Impact on Regional Climate (EASTAIRC): an overview. *J Geophys Res* 116. doi:10.1029/2010JD015257
- Li Z, Lee KH, Wang Y, Xin J, Hao WM (2010) First observation-based estimates of cloud-free aerosol radiative forcing across China. *J Geophys Res* 115. doi:10.1029/2009JD013306
- Luo Y, Krueger SK, Mace GG, Xu KM (2003) Cirrus cloud properties from a cloud-resolving model simulation compared to cloud radar observations. *J Atmos Sci* 60:510–525
- Luo Y, Krueger SK, Moorthi S (2005) Cloud properties simulated by a single-column model. Part I: comparison to cloud radar observations of cirrus clouds. *J Atmos Sci* 62:1428–1445
- Mace GG, Benson S (2008) The vertical structure of cloud occurrence and radiative forcing at the SGP ARM Site as revealed by 8 years of continuous data. *J Clim* 21. doi:10.1175/2007JCLI1987.1
- Mace GG, Zhang Q, Vaughn M, Marchand R, Stephens G, Trepte C, Winker D (2009) A description of hydrometeor layer occurrence statistics derived from the first year of merged Cloudsat and CALIPSO data. *J Geophys Res* 114. doi:10.1029/2007JD009755
- Marchand RT, Ackerman TP, King MD, Moroney C, Davies R, Muller JP, Gerber H (2001) Multiangle observations of arctic clouds from FIRE ACE: June 3, 1998, case study. *J Geophys Res* 106:15201–15214
- Miller MA (2008) The cloud and land surface interaction campaign (CLASIC). *EOS Trans AGU* 89 Abstract H43D-03
- Miller MA, Johnson KL, Troyan DT, Clothiaux EE, Mlawer EJ, Mace GG (2003) ARM value-added cloud products: description and status. http://www.arm.gov/publications/proceedings/conf13/extended_abs/miller-ma.pdf
- Minnis P, Yi Y, Huang J, Ayers JK (2005) Relationships between radiosonde and RUC-2 meteorological conditions and cloud occurrence determined from ARM data. *J Geophys Res* 110. doi:10.1029/2005JD006005
- Moran KP, Martner BE, Post MJ, Kropfli RA, Welsh DC, Widener KB (1998) An unattended cloud-profiling radar for use in climate research. *Bull Am Meteor Soc* 79:443–455
- Naud C, Muller JP, Clothiaux EE (2003) Comparison between active sensor and radiosonde cloud boundaries over the ARM Southern Great Plains site. *J Geophys Res* 108. doi:10.1029/2002JD002887
- Okamoto H, Nishizawa T, Takemura T, Sato K, Kumagai H, Ohno Y, Sugimoto N, Shimizu A, Matsui I, Nakajima T (2008) Vertical cloud properties in the tropical western Pacific Ocean: validation of the CCSR/NIES/FRCGC GCM by shipborne radar and lidar. *J Geophys Res* 113. doi:10.1029/2008JD009812
- Protat A, Young SA, McFarlane S, L'Ecuyer T, Mace GG, Comstock J, Long JC, Berry E, Delanoë J (2014) Reconciling ground-based and space-based estimates of the frequency of occurrence and radiative effect of clouds around Darwin, Australia. *J Appl Meteor Clim* 53:456–478. doi:10.1175/JAMC-D-13-072.1
- Qian Y, Long CN, Wang H, Comstock JM, McFarlane SA, Xie S (2012) Evaluation of cloud fraction and its radiative effect simulated by IPCC AR4 global models against ARM surface observations. *Atmos Chem Phys* 12. doi:10.5194/acp-12-1785-2012
- Sela J (1980) Spectral modeling at the National Meteorological Center. *Mon Weather Rev* 108:1279–1292
- Stephens G (2005) Cloud feedbacks in the climate system: a critical review. *J Clim* 18:237–273
- Stephens G et al (2002) The CloudSat mission and the A-train. *Bull Am Meteor Soc* 83:1771–1790
- Thorsen TJ, Fu Q, Comstock JM, Sivaraman C, Vaughan MA, Winker DM, Turner DD (2013) Macrophysical properties of tropical cirrus clouds from the CALIPSO satellite and from ground-based micropulse and Raman lidars. *J Geophys Res* 118(16):9209–9220. doi:10.1002/jgrd.50691
- Tobin DC, Revercomb HE, Knuteson RO, Lesht BM, Strow LL, Hannon SE, Feltz WF, Moy LA, Fetzer EJ, Cress TS (2006) Atmospheric radiation measurement site atmospheric state best estimates for atmospheric infrared sounder temperature and water vapor retrieval validation. *J Geophys Res* 111. doi:10.1029/2005JD006103
- Wang J, Rossow WB (1995) Determination of cloud vertical structure from upper air observations. *J Appl Meteorol* 34:2243–2258
- Wang J, Rossow WB, Uttal T, Rozendaal M (1999) Variability of cloud vertical structure during ASTEX observed from a combination of rawinsonde, radar, ceilometer, and satellite. *Mon Weather Rev* 127:2482–2502
- Wang J, Rossow WB, Zhang Y (2000) Cloud vertical structure and its variations from a 20-year global rawinsonde dataset. *J Clim* 13:3041–3056
- Weare BC (1996) Evaluation of the vertical structure of zonally averaged cloudiness and its variability in the atmospheric model intercomparison project. *J Clim* 9:3419–3431
- Winker DM, Hunt WH, McGill MJ (2007) Initial performance assessment of CALIOP. *Geophys Res Lett* 34:L19803. doi:10.1029/2007GL030135
- Xi B, Dong X, Minnis P, Khaiyer M (2010) A 10-year climatology of cloud cover and vertical distribution derived from both surface and GOES observations over the DOE ARM SGP site. *J Geophys Res* 115. doi:10.1029/2009JD012800
- Xie SC, Zhang MH (2000) Analysis of the convection triggering condition in the NCAR CCM using ARM measurements. *J Geophys Res* 105:14983–14996
- Xu KM, Randall DA (1996) A semi-empirical cloudiness parameterization for use in climate models. *J Atmos Sci* 53:3084–3102
- Xu KM et al (2002) An intercomparison of cloud-resolving models with the ARM summer 1997 intensive observation period data. *Q J Roy Meteorol Soc* 128:593–624
- Yang F, Pan H, Krueger S, Moorthi S, Lord S (2006) Evaluation of the NCEP global forecast system at the ARM SGP site. *Mon Weather Rev* 134:3668–3690
- Yoo H, Li Z (2012) Evaluation of cloud properties in the NOAA/NCEP global forecast system using multiple satellite products. *Clim Dyn*. doi:10.1007/s00382-012-1430-0
- Yoo H, Li Z, You Y, Lord S, Weng F, Barker HW (2013) Diagnosis and testing of low-level cloud parameterizations for the NCEP/GFS model satellite and ground-based measurements. *Clim Dyn*. doi:10.1007/s00382-013-1884-8
- Zhang MH et al (2005) Comparing clouds and their seasonal variations in 10 atmospheric general circulation models with satellite measurements. *J Geophys Res* 110. doi:10.1029/2004JD005021
- Zhang Y, Klein SA (2010) Mechanisms affecting the transition from shallow to deep convection over land: inferences from observations of the diurnal cycle collected at the ARM Southern Great Plains site. *J Atmos Sci* 67:2943–2959
- Zhang J, Chen H, Li Z, Fan X, Peng L, Yu Y, Cribb M (2010) Analysis of cloud layer structure in Shouxian, China using RS92 radiosonde aided by 95 GHz cloud radar. *J Geophys Res* 115. doi:10.1029/2010JD014030
- Zhang J, Li Z, Chen H, Cribb M (2013) Validation of a radiosonde-based cloud layer detection method against a ground-based remote sensing method at multiple ARM sites. *J Geophys Res* 118. doi:10.1029/2012JD018515